

Finite Element Design of Rotor Permanent Magnet Flux Switching Machine with Arbitrary Slot, Pole and Phase Combinations

Dorđe M. Lekić and Slobodan N. Vukosavić

Abstract—A two-dimensional finite element approach for designing RPMFS (Rotor Permanent Magnet Flux Switching) machines is presented in this paper. The proposed method enables fast, accurate and computationally efficient assessment of different RPMFS machine designs with an arbitrary number of rotor poles, stator slots and stator phases. The appropriate stator winding layout is assembled for any feasible slot, pole and phase combination by employing the winding distribution table, which contributes to automating the design process. Based on the proposed method, a program is developed using the Octave FEMM (Finite Element Method Magnetics) toolbox. The program is suited for the use in the design stage, where it is necessary to determine various machine parameters for given core dimensions, terminal voltage constraints and adopted value of current density in the conductors, while taking iron saturation effects into account. Verification was carried out by simulating torque and EMF waveforms for several RPMFS machine designs.

Index Terms—Rotor permanent magnet flux switching machine, Octave, finite element method magnetics.

Original Research Paper
DOI: 10.7251/ELSI822093L

I. INTRODUCTION

ELECTRICAL machine design today is reemerging as one of the engineering disciplines that attracts wide attention of both the industrial and scientific community. This becomes evident after inspecting the literature on electrical machine design published just in the last decade [1], [2]. Advancements in the fields of computer simulation, mathematical modeling and optimization have lead to improvements in design of electrical machinery, increasing thereby the accuracy in prediction of machine performance and decreasing the costs of development in the design stage. In order to ensure market competitiveness, electrical machine manufacturers tend to reduce machine size for a given torque rating and to increase their efficiency, increasing the need for design optimization [1], [2]. In

addition, a variety of novel electrical machine topologies, especially permanent magnet synchronous machines (PMSMs) and new types of multiphase and fractional slot windings demand fast and accurate evaluation of different machine designs. While the use of empirically established analytical methods is limited to design of conventional machine topologies [3], most new types of electrical machines are designed by using Computer-Aided-Design tools (CAD). As most new types of electrical machines operate in conditions where the iron core is highly saturated, their design is, for the most part, based on FEA (Finite Element Analysis) [4].

Continuing the research conducted in [5] and [6], the authors of this paper present a two-dimensional finite element (FE) approach for designing RPMFS (Rotor Permanent Magnet Flux Switching) machines. RPMFS machines represent a relatively new concept of PMSMs, which were first proposed in [7]. The basic operation principle of the RPMFS machine is presented in [7] and [8]. In comparison to SPMFS (Stator Permanent Magnet Flux Switching) and IPM (Interior Permanent Magnet) machines with the same core dimensions, RPMFS machines feature higher torque density values and lower values of torque ripple [9]. These features make RPMFS machines suitable for use in traction applications, such as EVs (Electric Vehicles) and HEVs (Hybrid Electric Vehicles), where the space available for installing the machine is limited and where high torque density and low torque ripple are required. Furthermore, torque production of RPMFS machines is not significantly influenced by permanent magnet (PM) demagnetization, as opposed to SPMFS machines, where demagnetization reduces the value of average torque [10]. In [11] several RPMFS designs with fixed core dimensions and fixed number of stator slots, but with different number of rotor poles are analyzed, confirming that torque production of the RPMFS machine can be improved by selecting the appropriate number of rotor poles. It should be noted, however, that the number of stator slots per rotor pole has a high impact on machine cogging torque [12], which is a dominant part of torque ripple, making it an important issue for traction applications. Thus, a comprehensive analysis and design optimization must take different slot, pole and phase combinations into account. The process of assembling an appropriate stator winding for feasible slot, pole and phase combinations can be generalized and, to a certain extent, automated by employing the winding distribution table (WDT), which was first proposed in [13].

Manuscript received 14 November 2018. Received in revised form 5 December 2018. Accepted for publication 7 December 2018.

D. M. Lekić is a PhD student at the Faculty of Electrical Engineering, University of Belgrade, Belgrade, Serbia. He is currently with the Faculty of Electrical Engineering, University of Banja Luka, Banja Luka, Republika Srpska, Bosnia and Herzegovina (+387(51)221-868; fax: +387(51)221-820; e-mail: djordje.lekic@etf.unibl.org).

S. N. Vukosavić is with the Faculty of Electrical Engineering, University of Belgrade, Belgrade, Serbia. (e-mail: boban@etf.bg.ac.rs).

The main goal of this study is to develop a methodology for finite element based design of RPMFS machines which is not restricted to any specific values of core dimensions, number of rotor poles, stator slots or even stator phases, making it suitable for use in the design stage, for evaluating torque production and induced voltage quality, or in automated design optimization. The proposed method is implemented as a program in Octave software using the Octave FEMM toolbox [14], while femm 4.2 software is employed for FE simulations [15], [16]. The program workflow is shown in Fig. 1.

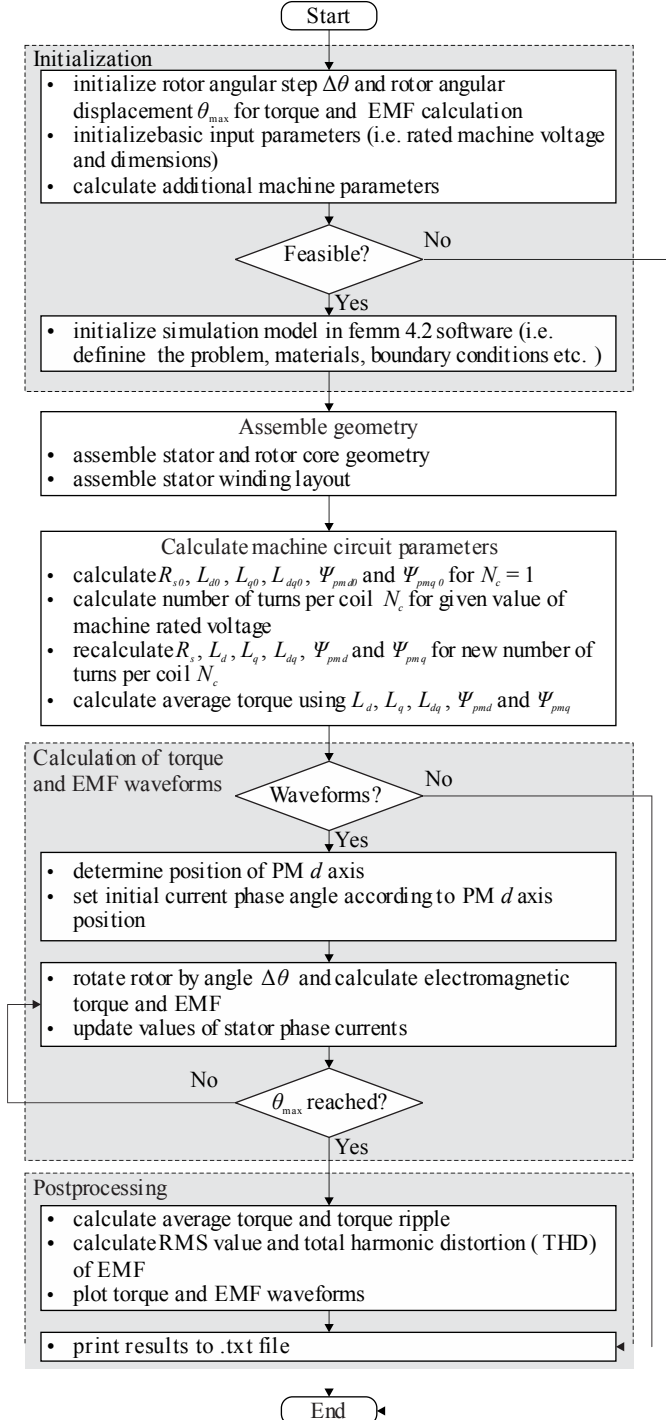


Fig. 1. Program workflow.

The organization of this paper resembles the program workflow shown in Fig. 1. In Section II the main input parameters are explained and the methodology for assembling the stator and rotor geometry, as well as the stator winding layout is presented. The algorithm for calculating machine circuit parameters such as resistances, inductances and flux linkages is given in Section III, while the methodology for obtaining electromagnetic torque and induced electromotive force (EMF) waveforms is presented in Section IV. Section V summarizes the results for several RPMFS designs with different number of slots, poles and phases, while general conclusions are given in Section VI.

II. ASSEMBLING RPMFS MACHINE MODEL

In this Section, the process for assembling the RPMFS machine model in femm 4.2 software will be explained. In order to get insight into the topology of the RPMFS machine, Fig. 2 shows an example of a 28-pole, 24-slot RPMFS machine. The stator is equipped with a single layer non-overlapping fractional slot winding. This type of stator winding consists of alternate tooth-wound coils which have short end windings, low values of resistances and copper losses, high values of slot fill factor, negligible values of coil mutual inductances and a high fault tolerance capability [18], [19]. While the stator has a conventional design, the construction of the rotor is somewhat special. From Fig. 2 it can be seen that the rotor magnetic circuit consists of so-called “rotor cells” which are placed on a non-magnetic support body [5]-[11]. Each rotor cell consists of a permanent magnet placed between two rotor teeth, whereas the rotor tooth tips form alternate magnetic poles. In this manner, one rotor cell represents one pole pair.

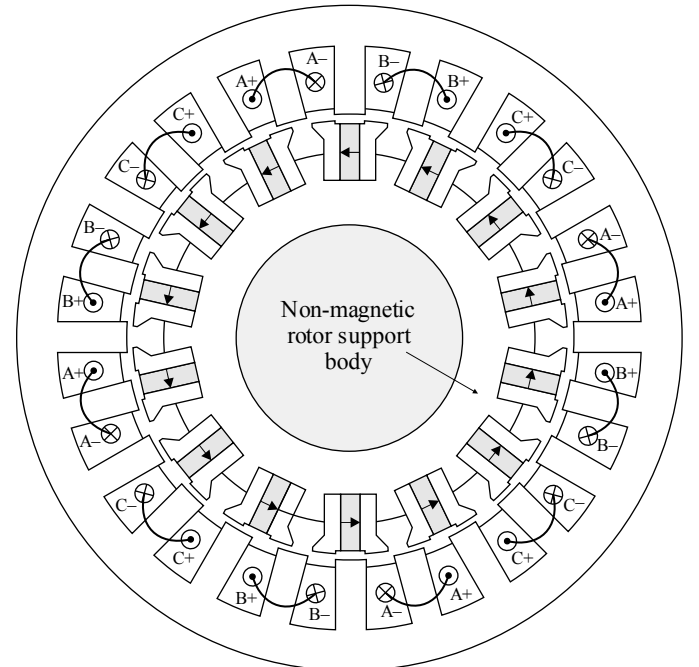


Fig. 2. Cross-section of a 28-pole, 24-slot RPMFS machine. The stator of the machine is equipped with a single layer non-overlapping fractional slot winding, consisting of 12 alternate tooth-wound coils. The rotor is equipped with 14 “rotor cells”, each containing 2 magnetic poles, placed on a non-magnetic support body [6].

A. Input Parameters

In the initialization part of the program, the values of following parameters are defined:

- number of stator slots – Q_s ;
- number of rotor poles – $2p$;
- number of stator winding phases – m ;
- number of stator winding layers – n_{lay} ;
- slot fill factor – k_{Cu} ;
- RMS value of rated phase voltage – U ;
- rated current density in the conductors – J ;
- rated rotor speed – n .

The last four parameters are defined for the purpose of EMF and torque calculation, while all other parameters are used for assembling stator and rotor geometry, as well as the stator winding layout. As will be explained in Section IV, the torque and EMF waveforms are obtained by rotating the rotor in steps $\Delta\theta$ over an angle θ_{max} , so that both these values are also defined in the initialization part of the program. The stator and rotor dimensions are defined according to Tables I and II, where the proposed ranges ensure reasonable machine designs. Only the stator outer diameter D_s , the stator lamination stack length l_s and the air-gap length δ_g are defined in meters, while all other dimensions are defined in relative units, as indicated in Tables I and II. In this manner, the program is not restricted to one particular set of machine core dimensions and it is sufficient to redefine just the basic parameters (D_s , l_s and δ_g) in order to get a new set of machine core dimensions with the same mutual ratios. Also, defining the core dimensions in relative units makes the program more suited for implementation of algorithms for geometry optimization [17].

TABLE I
STATOR INPUT DIMENSIONS [5]

Parameter name	Range
Ratio of inner and outer diameter (split ratio)	$0.45 < d_s/D_s < 0.75$
Ratio of tooth width to slot pitch	$0.3 < b_{ts}/\tau_s < 0.7$
Ratio of slot opening width to slot pitch	$0.05 < b_{os}/\tau_s < 0.7$
Ratio of tooth height to difference of outer and inner radius	$0.4 < 2h_{ts}/(D_s - d_s) < 0.8$
Ratio of tooth tip height to difference of outer and inner radius	$0 < 2h_{os}/(D_s - d_s) < 0.1$

TABLE II
ROTOR INPUT DIMENSIONS [5]

Parameter name	Range
Ratio of inner and outer diameter (split ratio)	$0.45 < d_r/D_r < 0.75$
Ratio of tooth width to inner pole pitch	$0.3 < b_{tr}/\tau_r < 0.7$
Ratio of PM width to inner pole pitch	$0.3 < b_{pm}/\tau_r < 0.7$
Ratio of slot opening width to outer pole pitch	$0.3 < b_{or}/\tau_{or} < 0.7$
Ratio of pole width to outer pole pitch	$0.3 < b_p/\tau_{or} < 0.7$
Ratio of tooth tip height to difference of outer and inner radius	$0.05 < 2h_{or}/(D_r - d_r) < 0.1$

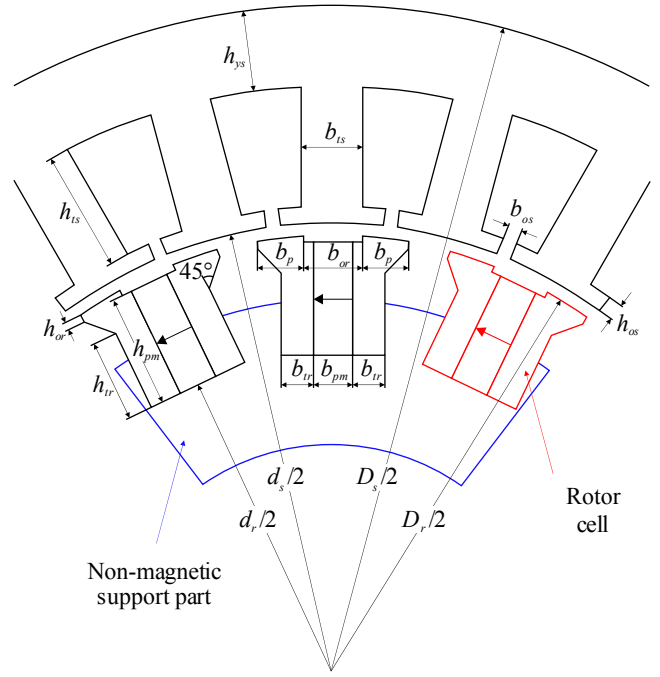


Fig. 3. A detail of a 28-pole, 24-slot RPMFS machine with main geometric design parameters [5].

Before assembling the simulation model in femm 4.2 software, the program checks the geometrical feasibility of the initialized parameters according to Table III. Geometrical feasibility implies that the initialized parameters correspond to a real machine geometry and that there is no overlapping of edges and no negative lengths [17]. If the initialized parameters pass the feasibility check, all stator and rotor dimensions are calculated in meters, respecting the topology shown in Fig. 3 and a finite element simulation model in femm 4.2 software is generated.

TABLE III
GEOMETRICAL FEASIBILITY CONDITIONS

Description	Mathematical formulation
The number of poles is even.	$\text{mod}(2p, 2) = 0$
The number of slots is divisible by the number of phases.	$\text{mod}(Q_s, m) = 0$
The number of slots is even for single-layer windings [18], [19].	$\text{mod}(Q_s, 2) = 0$ for $n_{lay} = 1$
The number of slots per phase is divisible by $t = \text{gcd}(Q_s, p)$ [18], [19].	$\text{mod}(Q_s / m / t, 1) = 0$
Sum of stator slot opening and stator tooth width is less than stator slot pitch.	$b_{ts} + b_{os} < \tau_s$
Sum of stator tooth height and stator tooth tip height is less than difference of outer and inner stator radius.	$h_{ts} + h_{os} < (D_s - d_s) / 2$
Sum of rotor tooth width and half of rotor permanent magnet width is less than rotor inner pole pitch.	$b_{tr} + b_{pm} / 2 < \tau_r$
Sum of rotor pole width and half of rotor slot opening width is less than rotor outer pole pitch.	$b_p + b_{or} / 2 < \tau_{or}$
Rotor permanent magnet width is less than rotor slot opening width.	$b_{pm} < b_{or}$

B. Stator and Rotor Geometry

In order to assemble stator and rotor geometry, one stator slot (Fig. 4a) and one rotor cell (Fig. 4b) are constructed first. The stator slot is copied Q_s/t times and the copies are equally distributed over the angle $2\pi/t$, where t is the machine periodicity, defined as the greatest common denominator (gcd) between Q_s and p , as follows [13]:

$$t = \text{gcd}(Q_s, p). \quad (1)$$

In a similar manner, the rotor cell is copied p/t times and the copies are again equally distributed over the angle $2\pi/t$. This means that the number of rotor poles and stator slots can be divided by their greatest common denominator in order to obtain the smallest segment of the machine that can be analyzed via symmetry [16]. For $t = 1$, the whole machine must be analyzed, while for $t > 1$, the machine can be divided in t segments and the results for the whole machine can be obtained by simulating only one out of t segments, reducing thereby the computational efforts.

After assembling the stator and rotor geometry, all stator slots are grouped (marked blue in Fig. 5) and all rotor cells are grouped (marked red in Fig. 5). For $t > 1$, end boundaries must be added to the stator (B2, B3, B14 and B15 in Fig. 5) and the rotor (B7, B8, B9 and B10 in Fig. 5) in order to enclose the areas that belong to the stator and rotor core. In order to enable the rotation of the rotor, four line segments are added to the model – two on the stator side of the air-gap (B4 and B13 in Fig. 5) and two on the rotor side of the air-gap (B6 and B11 in Fig. 5). These line segments are disconnected at the middle of the air-gap. Later on, when the rotor is rotated, the end nodes of these segments will be connected with arcs (B5 and B12 in Fig. 5) on each step of the simulation, i.e. for each analyzed rotor position.

After defining all the boundaries, the boundary conditions are imposed according to Table IV. A Dirichlet boundary condition, with zero value of magnetic vector potential ($A_z = 0$), is assigned to the stator outer boundary (B1 in Fig. 5), while (anti)periodic boundary conditions are assigned to appropriate pairs of boundaries from B2 to B15. A periodic boundary condition joins two boundaries together, whereas the boundary values on corresponding points of the two boundaries are set equal to each other [15]. In the case of an antiperiodic boundary condition, the boundary values on corresponding points of the two joint boundaries are made to be of equal magnitude but opposite sign [15]. Whether periodic or antiperiodic boundaries will be applied, depends on the number of rotor poles and on the value of machine periodicity t . If the number of rotor poles to be analyzed p/t is odd, antiperiodic boundary conditions should be used [16]. Otherwise, if p/t is even, periodic boundary conditions should be used instead [16].

Finally, the materials that will be used in the simulation are defined and assigned to appropriate enclosed areas in the model. The materials are chosen from the femm 4.2 material library [15] amongst which are air, iron, PM and conductor material, as is indicated in Fig. 5 and Table V.

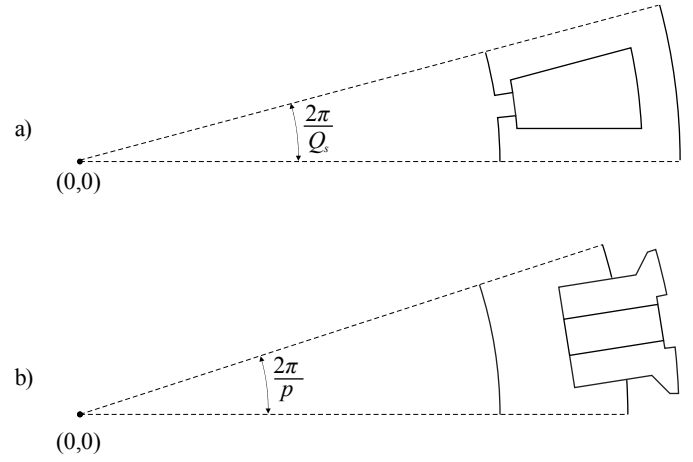


Fig. 4. a) Stator slot and b) rotor cell. The stator slot is copied Q_s/t times and the copies are equally distributed over the angle $2\pi/t$, where t is the machine periodicity. In a similar manner, the rotor cell is copied p/t times and the copies are again equally distributed over the angle $2\pi/t$ [5].

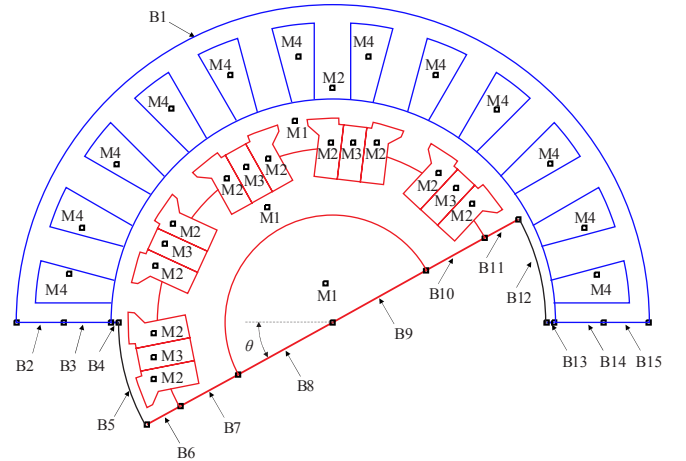


Fig. 5. Defining boundaries, boundary conditions and materials for an example 24-slot, 20-pole RPMFS machine. Only one half of the machine can be simulated in order to obtain results for the whole machine, because $t = \text{gcd}(24,10) = 2$ [5].

TABLE IV
BOUNDARY CONDITIONS

Boundary	Boundary condition
B1	Dirichlet (Zero magnetic vector potential)
B2, B15	(Anti)periodic 1
B3, B14	(Anti)periodic 2
B4, B13	(Anti)periodic 3
B5, B12	(Anti)periodic 4
B6, B11	(Anti)periodic 5
B7, B10	(Anti)periodic 6
B8, B9	(Anti)periodic 7

TABLE V
MATERIALS

Material name	Material type
M1	Air
M2	Iron (e.g. M-19 Steel)
M3	Permanent magnet (e.g. NdFeB 32 MGOe)
M4	Conductor (e.g. Copper)

C. Stator Winding Layout

The function for assembling the stator winding is based on the construction of the so-called WDT (Winding Distribution Table), which is a winding diagram representation in matrix form [13]. Each row in the WDT corresponds to one machine phase, while the number of columns is equal to the number of slots per phase ($n_c = Q_s/m$), according to Table VI [13].

TABLE VI
ORDER OF THE WDT ELEMENTS [13]

	column 1	column 2	...	column n_c
row 1	1	2	...	n_c
row 2	$n_c + 1$	$n_c + 2$...	$2n_c$
row 3	$2n_c + 1$	$2n_c + 2$...	$3n_c$
⋮	⋮	⋮	⋮	⋮
row m	$(m-1)n_c + 1$	$(m-1)n_c + 2$...	$m \cdot n_c$

The procedure for assembling the WDT is derived in [13], while only the key steps will be explained here. In the first step of the procedure, numbers are assigned to all stator slots. Starting from the first slot, the WDT is populated row by row, according to the progressive numbering illustrated in Table VI. The first slot number is assigned to the first element of the WDT. The second slot number is assigned to the WDT element whose distance is equal to p elements from the first one; the third slot number is assigned to the element whose distance is equal to p elements from the second one, and so on. When the element at position $Q_s = m \cdot n_c$ of the WDT is counted, the counting continues from the first element of the WDT. If the count ends in a filled cell, the adjacent empty cell is filled with the counted slot number. The procedure continues until the WDT is completely populated by stator slot numbers.

In order to visualize all positive and all negative phasors of the same phase in the same row, the WDT is further modified, depending on the phase number. For radially symmetrical (normal) polyphase systems, the last $\lfloor n_c/2 \rfloor$ WDT columns are shifted up by [13]:

$$\gamma = \begin{cases} \frac{m-1}{2}, & \text{for odd } m \\ \frac{m}{2} - 1, & \text{for even } m \end{cases} \quad (2)$$

rows (see Fig. 6a). In addition, a minus sign is added to the shifted columns, so that the coil sides with negative phasors can be identified [13]. For reduced polyphase systems, the rows are not shifted, but the second and third quadrants in Fig. 6b are swapped and the rows are reordered as in Table VII [13]. The sign of slot numbers in the third and fourth quadrant are then changed to account for negative coil sides [13].

TABLE VII
REORDERING WDT ROWS IN REDUCED SYSTEMS [13]

	1	2	...	n_c		1	2	...	n_c
1	⇒	1
2		$m/2 + 1$
⋮	⋮	⋮	⋮	⋮		2
$m/2$		$m/2 + 2$
$m/2 + 1$		⋮	⋮	⋮	⋮
⋮	⋮	⋮	⋮	⋮		$m/2$
m		m

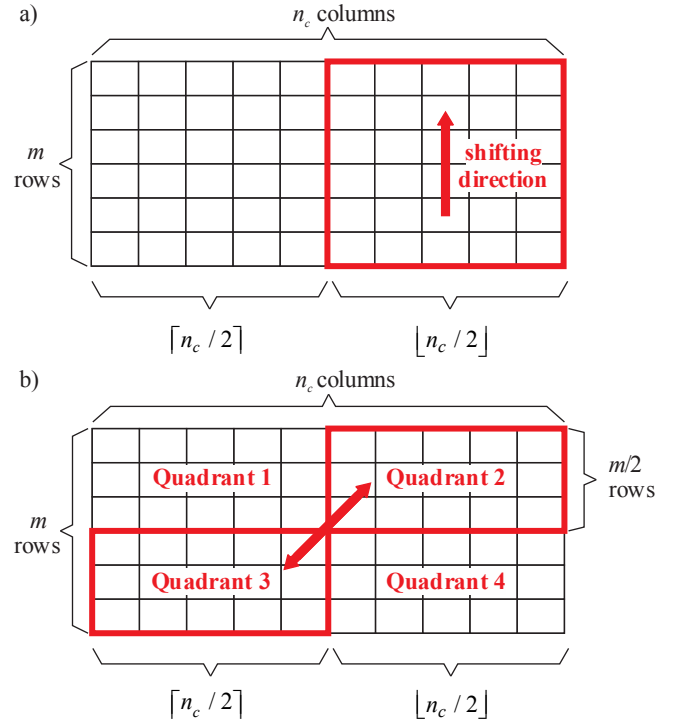


Fig. 6. Modification of the WDT for a) radially symmetrical (normal) and b) reduced polyphase systems [5].

Reduced systems, whose number of phases is not a power of two, are composed of m_g groups of m_u -phase systems, shifted by an angle π/m , where m_g is the greatest prime factor of m and $m_u = m/m_g$ [13]. A typical example would be a reduced six phase system, which consists of $m_g = 2$ three-phase systems shifted by an angle of $\pi/6$ radians (see Fig. 20). The even groups of WDT rows (third and fourth row, seventh and eighth row etc.) must be multiplied by -1 in order to make these systems radially symmetrical and to avoid the use of a neutral line [13]. In the case of single-layer windings ($n_{lay} = 1$), the WDT elements are referred to phasors associated to each slot, i.e. to each coil side [13]. In double-layer windings ($n_{lay} = 2$), the WDT elements are referred to one coil side, whereas the second coil side position is defined by the coil pitch given as a number of stator slots [20]:

$$y_c = \text{round}\left(\frac{Q_s}{2p}\right). \quad (3)$$

In order to demonstrate this procedure, the WDT for a three-phase, 24-slot, 20-pole RPMFS machine is assembled and shown as Table VIII. From Table VIII, the stator winding layout for the case of a single-layer winding is formed according to Fig. 7a, where only one half of the machine is shown.

TABLE VIII
WDT FOR RPMFS MACHINE SHOWN IN FIG. 7 [5]

1	13	6	18	-7	-19	-12	-24
9	21	2	14	-3	-15	-8	-20
5	17	10	22	-11	-23	-4	-16

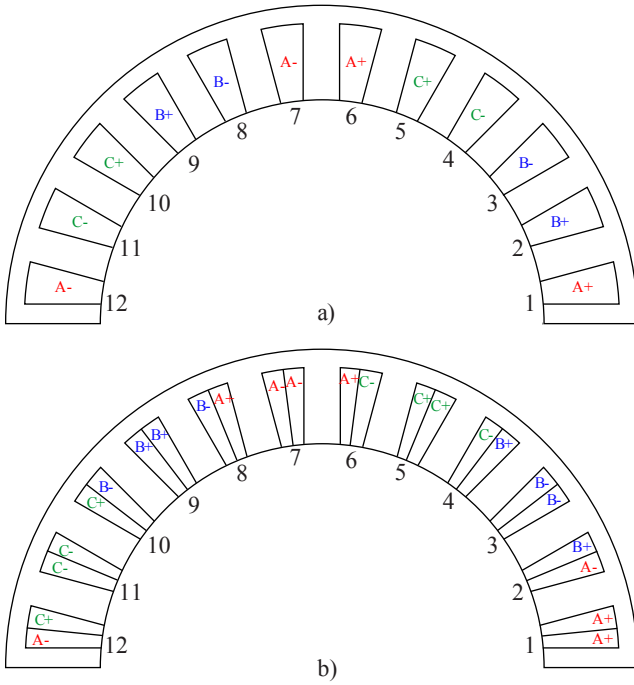


Fig. 7. Stator winding layout for an example three-phase, 24-slot, 20-pole RPMFS machine with a) single-layer and b) double-layer winding with a coil pitch of one slot ($y_c = 1$) [5].

From Fig. 7a it can be seen that, for example, coil sides in slots 1, 6, 7 and 12 belong to phase A winding. Positive phase A current exists in coil sides located in slots 1 and 6, because these slot numbers are denoted as positive in Table VIII. Negative phase A current exists in coil sides located in slots 7 and 12, because these slot numbers are denoted as negative in Table VIII. The same WDT is used when assembling a double-layer winding. From Fig. 7b it can be seen that, for the case of a double-layer winding, one coil side in each of the slots 1, 6, 7 and 12 belongs to phase A winding. Because the coil pitch for this example is $y_c = 1$, one coil side in each of the slots $1 + y_c = 2$, $6 + y_c = 7$, $7 + y_c = 8$ and $12 + y_c = 13$ also belongs to phase A, whereas the sign of the current is opposite to that in coil sides located in slots 1, 6, 7 and 12, respectively. The same analysis can be carried out for phases B and C.

III. CALCULATING RPMFS MACHINE PARAMETERS

In this Section, the process of calculating the circuit parameters of the assembled RPMFS machine model will be explained. Based on the methodology presented in [21], all parameters are first calculated assuming one turn per stator coil. After obtaining the values of all circuit parameters for one turn per coil, the corrected number of turns per coil N_c is calculated considering the fact that the sum of the d -axis and q -axis back electromotive forces and all voltage drops at rated speed n and rated current I has to equal the rated voltage U . All circuit parameters are then recalculated using the newly obtained number of turns per coil. In the remainder of this Section the values of parameters which are calculated for one turn per coil will be denoted with subscript 0, while their recalculated final values won't be denoted with any subscript.

A. Machine Inductances and Flux Linkages

In order to take the iron saturation at rated conditions into account, machine inductances and flux linkages are obtained by employing the frozen permeability method in femm 4.2 software. The frozen permeability method, which is described in [21] and [22], implies that several magnetostatic simulations are performed with constant values of iron permeability in the nodes of the finite element mesh. These permeabilities are determined for the rated operating point and are used in order to preserve information about the iron saturation at rated conditions. After “freezing” the permeability in this manner, the problem becomes linear and the circuit parameters can be determined one at a time, using the principle of superposition.

In [5]-[11] it has been shown that RPMFS machines are supplied with sinusoidal currents and that they have negligible reluctance torque, which means that maximum torque for given amplitudes of phase currents is obtained with zero d axis current. Thus, when simulating the rated operation, d axis current is set to zero, while q axis current is set to rated current. As the number of turns per coil N_c and the RMS value of rated stator current I are not known, the number of ampere-turns per stator coil is calculated first [21]:

$$N_c I = \frac{k_{Cu} J A_s}{n_{lay}}, \quad (4)$$

where the slot area is determined from stator core dimensions:

$$A_s = \frac{\pi}{4Q_s} \left[(D_s - 2h_{ys})^2 - (d_s + 2h_{os})^2 \right] - b_{is} h_{is}. \quad (5)$$

In (4) it is assumed that there is only one current path, but in applications where the rated current is specified in addition to the rated voltage, a method presented in [23] can be used for further fine tuning of the number of turns and number of parallel paths. The separation of the number of turns per coil N_c and of the RMS value of rated stator current I doesn't influence the results obtained for the magnetic field, meaning that magnetostatic simulations can be performed assuming $N_c = 1$.

Before calculating any parameters, the position of the d axis of the PMs relative to phase A axis must be determined. First, stator phase currents are set to zero and PMs are magnetized. Next, the RPMFS model is analyzed using femm 4.2 magnetics solver [14], [15] and the solution for z component of magnetic vector potential is obtained by solving Poisson's differential equation in the xy plane [4]:

$$-\frac{\partial}{\partial x} \left(\frac{1}{\mu_r} \frac{\partial A_z}{\partial x} \right) - \frac{\partial}{\partial y} \left(\frac{1}{\mu_r} \frac{\partial A_z}{\partial y} \right) = \mu_0 J_z. \quad (6)$$

In (6), μ_0 is the permeability of free space, μ_r is the relative permeability, J_z is the z component of current density vector, while A_z is the z component of magnetic vector potential. From the solution for A_z , the flux linkage for each phase winding is calculated [4]:

$$\psi_k = \frac{N_k I_s}{S_k} \left(\int_{\Omega_k^+} A_z d\Omega - \int_{\Omega_k^-} A_z d\Omega \right), \quad (k = 1, 2, \dots, m). \quad (7)$$

In (7), N_k is the number of turns in phase k winding, l_s is the stator stack length, S_k is the cross-sectional area of all coil sides belonging to phase k winding, while Ω_k^+ and Ω_k^- represent the areas with positive and negative phase k current. Assuming that the d axis of the PMs is aligned with phase A axis, the d and q axis flux linkages are calculated as [24]:

$$\psi_d = \frac{2}{m} \sum_{k=1}^m \psi_k \cos \left[(k-1) \frac{2\pi}{m} \right], \quad (8)$$

$$\psi_q = \frac{2}{m} \sum_{k=1}^m \psi_k \sin \left[(k-1) \frac{2\pi}{m} \right], \quad (9)$$

where the amplitude invariant form of the Park transformation is employed. After calculating d and q axis flux linkages, the electrical angle α between stator phase A axis and PM d axis is obtained from Fig. 8 as [5]:

$$\alpha = \text{atan} \left(\frac{\psi_q}{\psi_d} \right). \quad (10)$$

For given values of currents i_d and i_q , stator phase currents are calculated as [24]:

$$i_k = i_d \cos \left[\theta - (k-1) \frac{2\pi}{m} \right] + i_q \sin \left[\theta - (k-1) \frac{2\pi}{m} \right], \quad (k=1, 2, \dots, m). \quad (11)$$

With initial rotor position set to $\theta = \alpha$ and with $i_d = 0$, the stator winding is supplied with following currents [5], [24]:

$$i_k = -\sqrt{2}I \sin \left[\alpha - (k-1) \frac{2\pi}{m} \right], \quad (k=1, 2, \dots, m), \quad (12)$$

where I is the RMS value of rated current, which is obtained from (4) assuming $N_c = 1$. With these values of stator phase currents and with PMs magnetized, another nonlinear magnetostatic simulation is performed in order to obtain the values of permeabilities in the nodes of the finite element mesh which correspond to rated RPMFS machine operation (Fig. 9). The values of “frozen” permeabilities are used to conduct three linear magnetostatic simulations from which the parameters Ψ_{pmd0} , Ψ_{pmq0} , L_{d0} , L_{q0} and $L_{qd0} = L_{dq0}$ are determined.

The first linear simulation is conducted by setting the stator currents to zero and leaving the PMs magnetized. The flux linkages of all phase windings are then calculated using the obtained solution for magnetic vector potential (Fig. 10), according to (6), and the d and q axis flux linkages are then calculated as [24]:

$$\psi_{pmd0} = \frac{2}{m} \sum_{k=1}^m \psi_k \cos \left[\alpha - (k-1) \frac{2\pi}{m} \right], \quad (13)$$

$$\psi_{pmq0} = -\frac{2}{m} \sum_{k=1}^m \psi_k \sin \left[\alpha - (k-1) \frac{2\pi}{m} \right]. \quad (14)$$

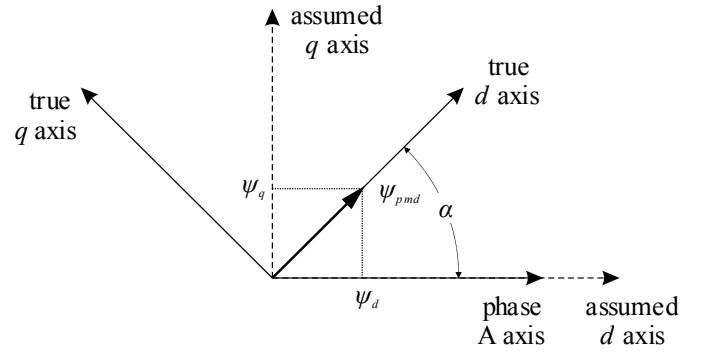


Fig. 8. Determining the relative position of phase A axis and PM d -axis.

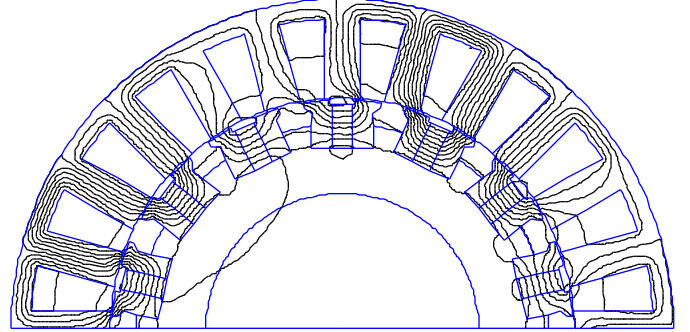


Fig. 9. Contour plot of magnetic vector potential for rated operating point of an example three-phase, 24-slot, 28-pole RPMFS machine, used to obtain “frozen” permeabilities for subsequent magnetostatic simulations.

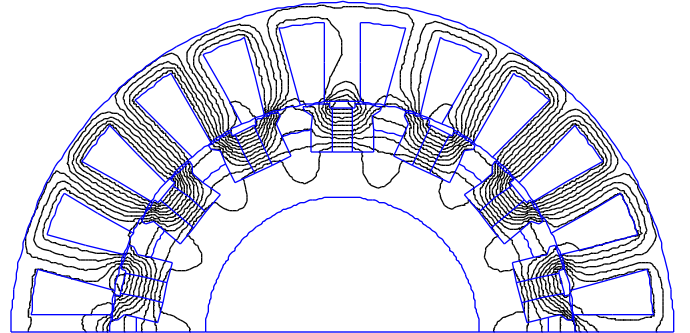


Fig. 10. Contour plot of magnetic vector potential for an example three-phase, 24-slot, 28-pole RPMFS machine with stator current set to zero and with PMs magnetized, used to obtain saturated values of Ψ_{pmd0} and Ψ_{pmq0} .

The flux linkage $\Psi_{pmd0} = \psi_{pmd0} / \sqrt{2}$ represents the RMS value of d axis flux linkage due to permanent magnets only, while $\Psi_{pmq0} = \psi_{pmq0} / \sqrt{2}$ is RMS value of q axis flux linkage due to PMs only, both calculated for one turn per stator coil. Although Ψ_{pmq0} is expected to be zero, because the flux of the PMs is expected to be aligned with d axis, Ψ_{pmq0} will nevertheless have a small non-zero value for the RPMFS machine, which is a consequence of the cross-saturation effect [21].

The second linear simulation is conducted by demagnetizing the PMs and setting the q axis current to zero ($i_q = 0$), while the d axis current can be set to an arbitrary value i_d , resulting in following stator currents [24]:

$$i_k = i_d \cos \left[\alpha - (k-1) \frac{2\pi}{m} \right], \quad (k=1, 2, \dots, m). \quad (15)$$

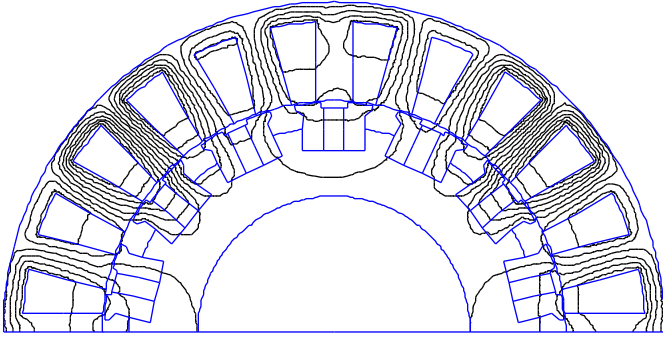


Fig. 11. Contour plot of magnetic vector potential for an example three-phase, 24-slot, 28-pole RPMFS machine with stator q -axis current set to zero and with PMs demagnetized, used to obtain saturated values of L_{d0} and L_{dq0} .

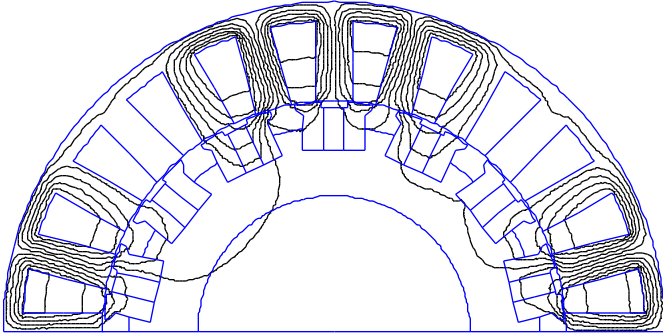


Fig. 12. Contour plot of magnetic vector potential for an example three-phase, 24-slot, 28-pole RPMFS machine with stator d -axis current set to zero and with PMs demagnetized, used to obtain saturated values of L_{q0} and L_{dq0} .

The corresponding flux linkages of all phase windings are then calculated using the obtained solution for magnetic vector potential (Fig. 11), according to (6), and flux linkages ψ_{d0} and ψ_{q0} are calculated as in (13) and (14). The saturated values of the d axis inductance and the cross-saturation inductance for one turn per stator coil are calculated as [21]:

$$L_{d0} = \frac{\Psi_{d0}}{i_d}, \quad L_{dq0} = \frac{\Psi_{q0}}{i_d}. \quad (16)$$

Finally, the last linear simulation is conducted by leaving the PMs demagnetized and setting the d axis current to zero ($i_d = 0$), while the q axis current can be set to an arbitrary value i_q , resulting in following stator currents [24]:

$$i_k = -i_q \sin \left[\alpha - (k-1) \frac{2\pi}{m} \right], \quad (k=1, 2, \dots, m). \quad (17)$$

The corresponding flux linkages of all phase windings are again calculated using the obtained solution for magnetic vector potential (Fig. 12), according to (6), and flux linkages ψ_{d0} and ψ_{q0} are calculated as in (13) and (14). The saturated values of the q axis inductance and the cross-saturation inductance for one turn per stator coil are calculated as [21]:

$$L_{q0} = \frac{\Psi_{q0}}{i_q}, \quad L_{dq0} = \frac{\Psi_{d0}}{i_q}. \quad (18)$$

It should be noted that $L_{qd0} = L_{dq0}$ [21] and $L_{d0} \approx L_{q0}$ [9], which can be confirmed by comparing the results of the last

two linear simulations. The end winding leakages are neglected in this calculation, which is in most cases justified because of short end windings of the RPMFS machine. However, for some combinations of stator slots, poles and phases, which may result in distributed, rather than tooth wound stator windings, this assumption has to be tested first.

B. Stator Winding Resistance

The stator winding resistance for one turn per coil is calculated as [21]:

$$R_{s0} = \rho_{Cu75} \frac{n_{lay}^2 l_c Q_s}{m k_{Cu} A_s}, \quad (19)$$

where $\rho_{Cu75} = 0,0216 \Omega \text{mm}^2/\text{m}$ is the resistivity of copper at temperature 75°C and $l_c = 2(l_s + l_{ew})$ is the coil length. The end winding length is calculated assuming semicircular end windings and taking the coil pitch y_c into account by following equation [20]:

$$l_{ew} = \frac{\pi}{4} (\tau_{s1/2} + b_{ts}) + 1,8 \tau_{s1/2} (y_c - 1), \quad (20)$$

where $\tau_{s1/2} = \pi(D_s + h_{st})/Q_s$ is the slot pitch measured at half of the stator tooth height.

C. Number of Turns per Coil

The number of turns per coil N_c is calculated considering the fact that the sum of the d -axis and q -axis back electromotive forces and all voltage drops at rated speed n and rated current I has to be equal to the rated voltage U . The phasor diagram for the rated operating point of the RPMFS machine is shown in Fig. 13, where currents, voltages and flux linkages are represented by their RMS values. It is assumed that the RPMFS machine is vector controlled with $I_d = 0$ and $I_q = I$, where I is the RMS value of rated current. The d and q axis components of rated stator voltage are [25]:

$$U_d = E_d + X_q I_q = \omega \Psi_{pmq} + \omega L_q I_q, \quad (21)$$

$$U_q = E_q + X_{dq} I_q + R_s I_q = \omega \Psi_{pmd} + \omega L_{dq} I_q + R_s I_q, \quad (22)$$

where $E_d = \omega \Psi_{pmq}$, $E_q = \omega \Psi_{pmd}$, $X_q = \omega L_q$ and $X_{dq} = \omega L_{dq}$. The angular frequency ω corresponds to rated rotor speed n .

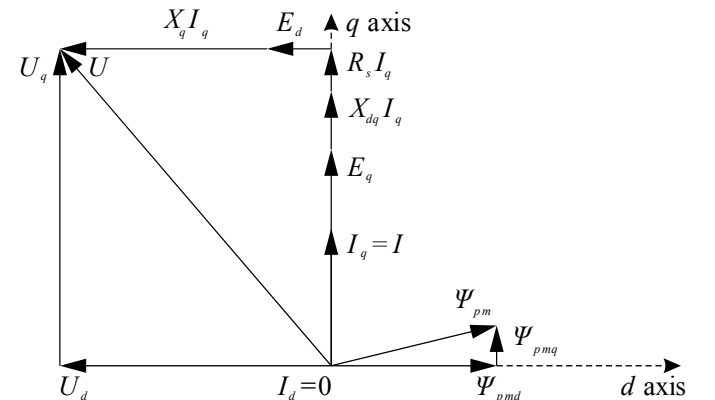


Fig. 13. Phasor diagram of the RPMFS machine which is vector controlled with $I_d = 0$ and $I_q = I$. Cross-saturation is modeled by X_{dq} , Ψ_{pmq} and E_d .

As the flux linkages are proportional to the number of turns per coil, while inductances and resistances are proportional to the square of the number of turns per coil, following equations are valid [21]:

$$\begin{aligned}\Psi_{pmd} &= N_c \Psi_{pmd0}, \\ \Psi_{pmq} &= N_c \Psi_{pmq0}, \\ L_d &= N_c^2 L_{d0}, \\ L_q &= N_c^2 L_{q0}, \\ L_{dq} &= N_c^2 L_{dq0}, \\ R_s &= N_c^2 R_{s0}.\end{aligned}\quad (23)$$

By substituting (23) into (21) and (22), we obtain:

$$U_d = \omega N_c \Psi_{pmq0} + \omega N_c L_{q0} N_c I_q, \quad (24)$$

$$U_q = \omega N_c \Psi_{pmd0} + \omega N_c L_{dq0} N_c I_q + N_c R_{s0} N_c I_q. \quad (25)$$

Taking into account that, for the amplitude invariant form of the Park transformation, following equations are valid:

$$N_c I_q = N_c I, \quad (26)$$

$$U = \sqrt{U_d^2 + U_q^2}, \quad (27)$$

we finally get the expression for calculating the number of turns per coil for given value of rated angular frequency ω , RMS value of rated voltage U and RMS value of rated ampere-turns per stator coil $N_c I$:

$$N_c = \frac{U/\omega}{\sqrt{\left(\Psi_{pmd0} + L_{dq0} N_c I + \frac{R_{s0}}{\omega} N_c I\right)^2 + \left(\Psi_{pmq0} + L_{q0} N_c I\right)^2}}. \quad (28)$$

After calculating the number of coils per turn N_c in this manner, all circuit parameters are recalculated according to (23). Also, the RMS value of rated stator current I and the number of turns per coil N_c are separated according to the value of the rated ampere-turns per stator coil $N_c I$, which is derived from (4). It should be emphasized that the equations used in the analysis presented in this Section are based on the amplitude invariant form of the Park transformation.

IV. CALCULATING RPMFS MACHINE TORQUE AND EMF

The torque and EMF waveforms are derived by rotating the rotor in steps $\Delta\theta$ over an angle θ_{\max} . For each rotor position, the simulated machine segment is analyzed using femm 4.2 magnetics solver [15], [16] and the solution for z component of magnetic vector potential is obtained by solving (6). From the solution for A_z , the flux linkages are calculated for all phase windings according to (7) and torque and EMF is calculated for each rotor position.

A. Torque Waveform

The electromagnetic torque acting upon the rotor of the RPMFS machine is calculated by employing the weighted stress tensor volume integral [15], [16], according to following

equation [22]:

$$T_e = \frac{k_{Fe} l_s}{\mu_0} \int_0^{2\pi} r^2 B_n B_t d\theta, \quad (29)$$

where μ_0 is the permeability of free space, k_{Fe} is the iron stacking factor, l_s is the stator laminations axial length, r is the radius of the integration path, and B_n and B_t are the normal and tangential flux density components in the air gap, respectively. In femm 4.2 software, the torque is calculated by selecting all rotor blocks (marked red in Fig. 5) and by evaluating the integral (29) for each rotor position. The values of torque for each rotor position are then stored in an array for the purpose of post processing.

The above proposed method for torque calculation is used to obtain the torque waveform, from which the average torque and the torque ripple can both be derived. If torque ripple is not of interest, a more computationally efficient method can be used in order to calculate just the average value of torque. Based on the derivations in Section III, the average value of rated electromagnetic torque can be calculated as [21], [22]:

$$T_{avg} = 3p(\Psi_d I_q - \Psi_q I_d) = 3p \Psi_d I, \quad (30)$$

where the RMS value of d axis stator flux linkage is:

$$\Psi_d = \Psi_{pmd} + L_d I_d + L_{dq} I_q = \Psi_{pmd} + L_{dq} I, \quad (31)$$

and where $I_d = 0$ and $I_q = I$ is assumed. For some applications, such as torque density optimization of RPMFS machines, the second approach, based on just a few magnetostatic simulations, can be used because of its computational efficiency and acceptable accuracy. However, for applications where the torque ripple has to be optimized, the first approach, based on the torque waveform obtained from a series of magnetostatic simulations, has to be used.

B. EMF Waveform

The value of induced EMF in phase k is calculated by applying Faradays law for each rotor position θ during the simulation:

$$e_k(\theta) = \frac{p\pi}{30} n \frac{\psi_k(\theta) - \psi_k(\theta - \Delta\theta)}{\Delta\theta}, \quad (k = 1, 2, \dots, m), \quad (32)$$

where n is the value of rotor speed in rpm. The phase flux linkages in (32) are calculated according to (7). The values of phase EMFs for each rotor position are again stored in an array for the purpose of post processing.

V. PRESENTING THE RESULTS

The outputs of the program are plots of torque and phase EMF waveforms. In the post processing part of the program, the average value of machine torque and the value of torque ripple are calculated and shown as data on these plots. The program also performs harmonic analysis of EMF waveforms and calculates the RMS value of the fundamental harmonic and the total harmonic distortion (THD) of the induced phase EMF. Machine output parameters are printed to a text file.

In order to demonstrate the form of the results, three RPMFS machines with different numbers of slots, poles and phases are simulated, according to input parameters given in Table IX. All other input parameters are adopted according to Table X and they have the same values for all three analyzed RPMFS machines. It should be noted that these machine designs are in no way optimized and that they are used for demonstration purposes only. A relatively small value of the angular step $\Delta\theta$ is adopted in order to get smooth torque and EMF waveforms (accurate value of torque ripple and EMF harmonics), but a higher value could be adopted without significant loss of accuracy in calculated average torque. It should be noted that higher values of angular step $\Delta\theta$ would result in fewer magnetostatic simulations and, thus, in shorter overall computation time. This is important when the program is used as a part of an iterative optimization procedure, where the goal is to maximize the average torque for given machine volume (volume torque density). The mesh is automatically generated for each rotor position according to femm 4.2 software default settings [15], [16], which was shown to be appropriate for machine design purposes. The values of air-gap length, stator outer diameter and stator lamination stack length are adopted from [7] and [8]. The PM material used in simulations is N36Z2G, with data: $H_c = 846625$ A/m; $\mu_r = 1.165$; $B_r = \mu_r \cdot \mu_0 \cdot H_c = 1.24$ T [7], [26].

TABLE IX
INPUT PARAMETERS FOR THREE RPMFS MACHINES

Parameter name	Symbol	M1	M2	M3
Number of stator slots	Q_s	24	30	24
Number of rotor poles	$2p$	20	28	28
Number of stator winding phases	m	3	5	6
Number of stator winding layers	n_{lay}	1	1	2

TABLE X
COMMON INPUT PARAMETERS

Parameter name	Symbol	Value
Angular step in electrical degrees	$p \cdot \Delta\theta$	4
Total angular displacement of rotor in electrical degrees	$p \cdot \theta_{max}$	360
Rated RMS value of phase voltage, V	U	230
Rated RMS value of current density in the conductors, A/mm ²	J	5
Slot fill factor	k_{Cu}	0.68
Rotor speed, rpm	n	500
Air-gap length, mm	δ_g	0.73
Stator outer diameter, mm	D_s	269
Stator stack length, mm	l_s	83.56
Ratio of inner and outer stator diameter	d_s / D_s	0.7
Ratio of stator tooth width to slot pitch	b_{ts} / τ_s	0.6
Ratio of stator slot opening width to slot pitch	b_{os} / τ_s	0.4
Ratio of stator tooth height to difference of outer and inner stator radius	$2h_{ts} / (D_s - d_s)$	0.8
Ratio of stator tooth tip height to difference of outer and inner stator radius	$2h_{os} / (D_s - d_s)$	0
Ratio of inner and outer rotor diameter	d_r / D_r	0.7
Ratio of rotor tooth width to inner pole pitch	b_{tr} / τ_r	0.5
Ratio of PM width to rotor inner pole pitch	b_{pm} / τ_{ir}	0.5
Ratio of slot opening width to outer pole pitch	b_{or} / τ_{or}	0.5
Ratio of pole width to rotor outer pole pitch	b_p / τ_{or}	0.5
Ratio of tooth tip height to difference of outer and inner rotor radius	$2h_{or} / (D_r - d_r)$	0.1

The contour plots of magnetic vector potential for all three analyzed machines are shown in Fig. 14, 15 and 16, while the output parameters for all three machines are given in Table XI. The efficiency of the machines in Table XI is calculated by taking the copper losses into account, whereas the iron and mechanical losses are neglected, which must be reconsidered for some applications. The power factor is calculated by taking the voltage harmonics into account, while the currents are sinusoidal. In Table XI it can be seen that all three machines develop approximately the same average torque. This is mainly due to the same values of machine volume, current density in the conductors and approximately the same values of flux densities. The main difference between the machines is the torque ripple, which depends on the slot/pole combinations, and it is highest for machine M1. In Table XI it can also be verified that $L_d \approx L_q$ for all three designs, and that the cross-saturation parameters L_{dq} and Ψ_{pmq} have small negative values.

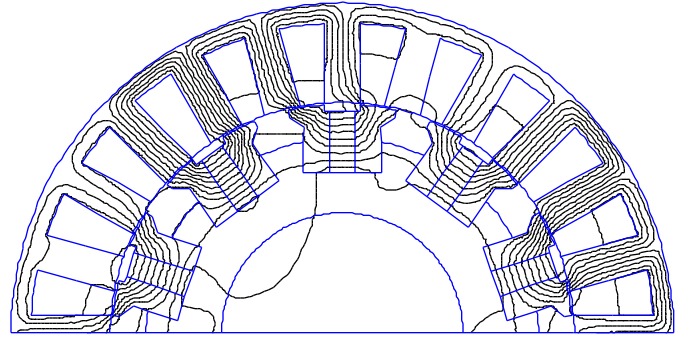


Fig. 14. Contour plot of magnetic vector potential for rated operation of machine M1 ($Q_s = 24$, $2p = 20$, $m = 3$, $n_{lay} = 1$).

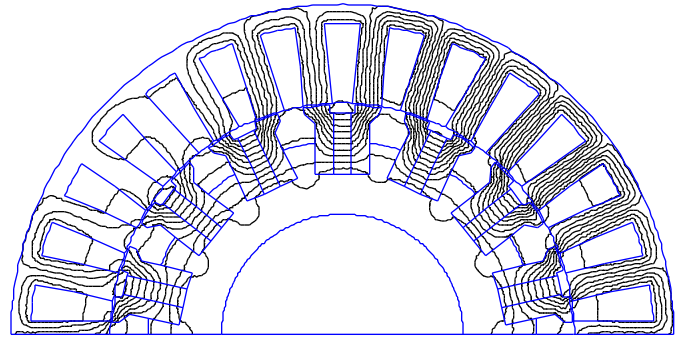


Fig. 15. Contour plot of magnetic vector potential for rated operation of machine M2 ($Q_s = 30$, $2p = 28$, $m = 5$, $n_{lay} = 1$).

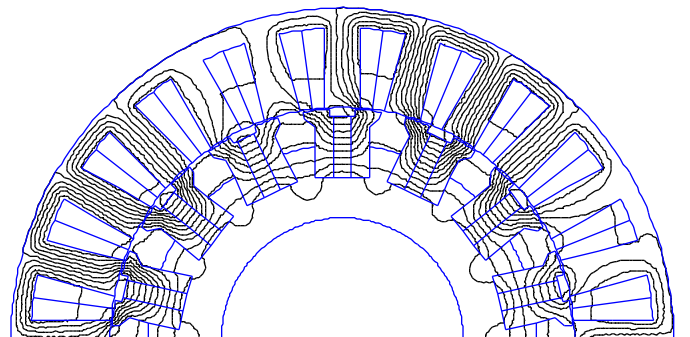


Fig. 16. Contour plot of magnetic vector potential for rated operation of machine M3 ($Q_s = 24$, $2p = 28$, $m = 6$, $n_{lay} = 2$).

TABLE XI
OUTPUT PARAMETERS FOR THREE RPMFS MACHINES

Parameter name	Symbol	M1	M2	M3
Mechanical output power, kW	P	10.5	11.2	11.3
RMS value of phase current, A	I	21	13.5	11.8
Power factor	PF	0.81	0.80	0.75
Efficiency	η	0.89	0.90	0.93
Average torque, Nm	T_{avg}	201	213	216
Torque ripple, %	T_{ripple}	7.53	1.08	2.68
Voltage harmonic distortion, %	THD _v %	12.43	9.98	4.12
Number of turns per coil	N_c	74	92	66
Stator winding resistance, Ω	R_s	1 Ω	1.3	1.1
d axis inductance, mH	L_d	14.3	16.7	20.8
q axis inductance, mH	L_q	14.0	16.1	20.5
Cross-saturation inductance, mH	L_{dq}	-0.6	-0.7	-0.8
d axis PM flux, mWb	Ψ_{pmd}	330	234	227
Cross-saturation PM flux, mWb	Ψ_{pmq}	-41	-30	-36
Tooth flux density, T	B_{is}	1.85	1.89	1.60
Yoke flux density, T	B_{ys}	1.71	1.28	1.31

The value of average torque presented in Table XI is calculated by solving the weighted stress tensor volume integral in femm 4.2 software for each rotor position and by calculating the mean value for all rotor positions. It is interesting to compare this result with the one obtained by inserting the values of parameters Ψ_{pmd} and L_{dq} in (30) and (31). For example, this calculation for machine M1 yields the following result:

$$T_{avg} = 3p(\Psi_{pmd}I + L_{dq}I^2) = 3 \cdot 10 \cdot (0.33 \cdot 21 - 0.0006 \cdot 21^2) \approx 200 \text{ Nm}, \quad (33)$$

which is very close to the value given in Table XI. This means that just the parameters Ψ_{pmd} and L_{dq} have to be determined by two magnetostatic simulations and then the average torque can be calculated analytically with good accuracy. The torque waveforms for all three machines are shown in Fig. 17, where the results from table XI can be verified. The phase EMF waveforms for all three analyzed machines are shown in Fig. 18, 19 and 20. It can be concluded that all three machines have radially symmetrical stator windings.

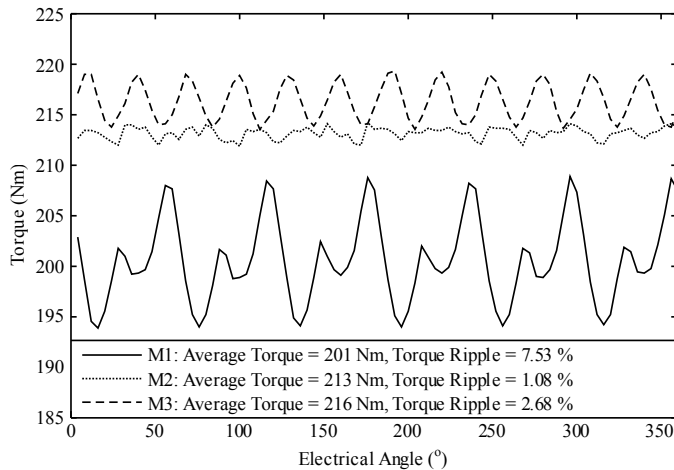


Fig. 17. Torque vs. electrical angle for analyzed RPMFS machines. Machine M1 has the lowest average value of torque and, at the same time, the highest value of torque ripple.

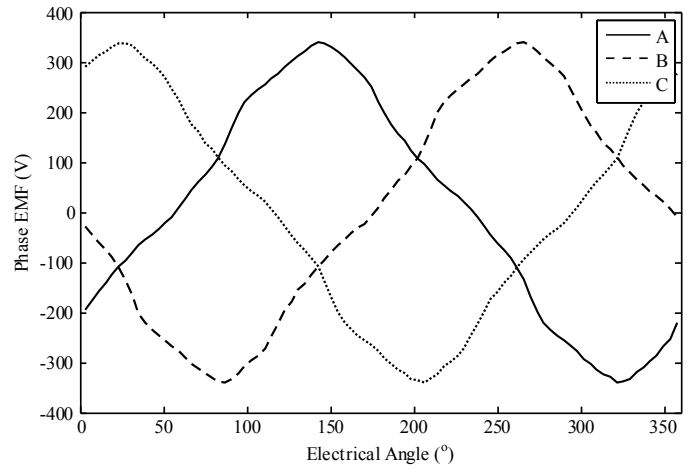


Fig. 18. Phase EMF vs. electrical angle for rated operation of machine M1 (Fundamental harmonic of phase EMF = 213.8 V, THD_v = 12.43 %).

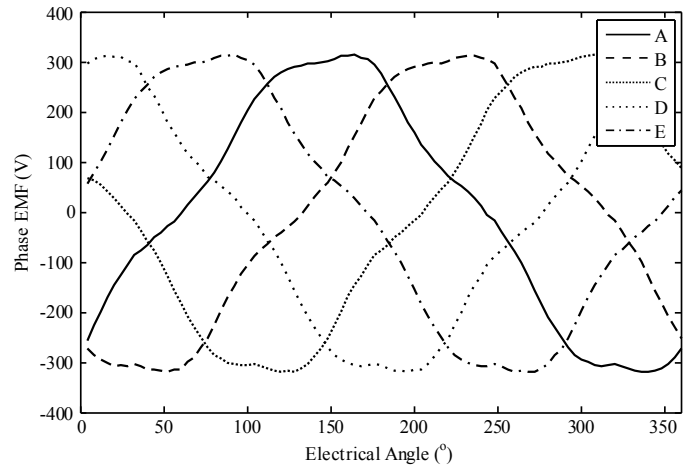


Fig. 19. Phase EMF vs. electrical angle for rated operation of machine M2 (Fundamental harmonic of phase EMF = 217.7 V, THD_v = 9.98 %).

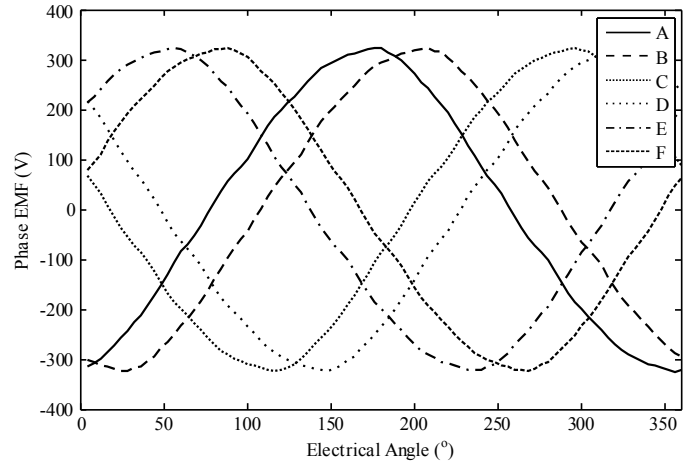


Fig. 20. Phase EMF vs. electrical angle for rated operation of machine M3 (Fundamental harmonic of phase EMF = 223.5 V, THD_v = 4.12 %). The phase EMFs for machine M3 are unevenly spaced in time, which is due to the fact that the stator winding is a reduced six-phase winding. The reduced six-phase system consists of two three-phase systems shifted by an angle of $\pi/6$ radians, whereas the first three-phase system consists of phases A, C and E, and the second three-phase system consists of phases B, D and F.

VI. CONCLUSION

The methodology for FE based design of RPMFS machines was presented in this paper, along with the corresponding application program, coded in Octave software FEMM toolbox. Guidelines for assembling the stator and rotor geometry, the stator winding layout, as well as calculation techniques for the machine circuit parameters, torque and EMF waveforms were developed and thoroughly explained respecting the procedures employed in the literature. The developed program enables fast and efficient analysis of RPMFS machines with different numbers of stator slots, stator phases, rotor poles and overall different dimensions. While the methodology presented in this paper is not restricted to RPMFS machines only, the program is intended to be used for geometry optimization of the RPMFS machine, with the aim of achieving maximum torque volume density and minimum torque ripple.

REFERENCES

- [1] G. Bramerdorfer, J. A. Tapia, J. J. Pyrhönen and A. Cavagnino, "Modern Electrical Machine Design Optimization: Techniques, Trends, and Best Practices," *IEEE Trans. Ind. Electron.*, vol. 65, no. 10, pp. 7672 - 7684, Feb. 2018.
- [2] Y. Duan and D. M. Ionel, "A Review of Recent Developments in Electrical Machine Design Optimization Methods With a Permanent-Magnet Synchronous Motor Benchmark Study," *IEEE Trans. Ind. Appl.*, vol. 49, no. 3, pp. 1268 - 1275, Mar. 2013.
- [3] J. Pyrhönen, T. Jokinen and V. Hrabecova, *Design of Rotating Electrical Machines*, Wiltshire: John Wiley & Sons, 2008.
- [4] S. Salon, *Finite Element Analysis of Electrical Machines*, Troy, New York: Springer, 1995.
- [5] Đ. Lekić and S. Vukosavić, "Program for Finite Element Based Design of Rotor Permanent Magnet Flux Switching Machine," in *2018 International Symposium on Industrial Electronics (INDEL)*, Banja Luka, Bosnia and Herzegovina, pp. 1-7, 1-3 Nov. 2018.
- [6] Đ. Lekić and S. Vukosavić, "Calculation of Optimal Rotor Permanent Magnet Dimensions for RPMFS Machine," in *INFOTEH-JAHORINA (INFOTEH), 2018 17th International Symposium*, East Sarajevo, Bosnia-Herzegovina, pp. 1-6, 21-23 March 2018.
- [7] W. Hua, P. Su, G. Zhang, M. Cheng, "A Novel Rotor-Permanent Magnet Flux-Switching Machine," in *Ecological Vehicles and Renewable Energies (EVER), 2015 Tenth International Conference on*, Monte Carlo, Monaco, pp. 1-10, 31 Mar. - 2 Apr. 2015.
- [8] P. Su, W. Hua, Z. Wu, P. Han and M. Cheng, "Analysis of the Operation Principle for Rotor-Permanent-Magnet Flux-Switching Machines," *IEEE Trans. Ind. Electron.*, vol. 65, no. 2, pp. 1062 - 1073, Feb. 2018.
- [9] P. Su, W. Hua, G. Zhang, Z. Chen, M. Cheng, "Analysis and Evaluation of Novel Rotor Permanent Magnet Flux-Switching Machine for EV and HEV Applications," *IET Electric Power Applications*, vol. 11, no. 9, pp. 1610-1618, Nov. 2017.
- [10] P. Su and W. Hua, "Performance comparison between rotor flux-switching and stator flux-switching machines considering local demagnetization," *AIP Advances*, pp. 1-5, vol. 7, Jan. 2017.
- [11] P. Su, W. Hua, C. Hou and M. Hu, "Research on the influence of rotor poles number on performances of rotor permanent-magnet flux-switching machines," in *2017 IEEE Energy Conversion Congress and Exposition (ECCE)*, Cincinnati, OH, USA, pp. 1-8, 1-5 Oct. 2017.
- [12] Z. Q. Zhu and D. Howe, "Influence of Design Parameters on Cogging Torque in Permanent Magnet Machines," *IEEE Trans. Energy Convers.*, vol. 15, no. 4, pp. 407-412, Dec. 2000.
- [13] M. Caruso, A. D. Tommaso, F. Marignetti, R. Miceli and G. Galluzzo, "A General Mathematical Formulation for Winding Layout Arrangement of Electrical Machines," *Energies*, vol. 11, no. 2, pp. 446-470, Feb. 2018.
- [14] D. Meeker, *Finite Element Method Magnetics: OctaveFEMM Version 1.2 User's Manual*, Oct. 2006.
- [15] D. Meeker, *Finite Element Method Magnetics Version 4.2 User's Manual*, Feb. 2009.
- [16] D. Meeker, "Finite Element Method Magnetics," 6 Apr. 2014. [Online]. Available: <http://www.femm.info>. [Accessed 10 6 2018].
- [17] S. Stipetić, W. Miebach and D. Žarko, "Optimization in Design of Electric Machines: Methodology and workflow," in *ACEMP-OPTIM-ELECTROMOTION 2015 Joint Conference*, Side, Turkey, pp. 1-8, 2-4 Sep. 2015.
- [18] N. Bianchi, M. Dai Pre, "Use of the Star of Slots in Designing Fractional-Slot Single-Layer Synchronous Motors," *IEE Proceedings - Electric Power Applications*, vol. 153, no. 3, pp. 459 - 466, May 2006.
- [19] N. Bianchi, S. Bolognani, M. Pre and G. Grezzani, "Design considerations for fractional-slot winding configurations of synchronous machines," *IEEE Trans. Ind. Appl.*, vol. 42, no. 4, pp. 997 - 1006, July 2006.
- [20] N. Bianchi, M. Pre, L. Alberti and E. Fornasiero, *Theory and Design of Fractional-Slot PM Machines*, Padova, Italy: CLEUP cp, Sep. 2007.
- [21] D. Žarko, D. Ban and R. Klarić, "Finite Element Approach to Calculation of Parameters of an Interior Permanent Magnet Motor," *Automatika: Journal for Control, Measurement, Electronics, Computing and Communications*, vol. 46, no. 3-4, pp. 113-122, Jan. 2006.
- [22] W. Q. Chu and Z. Q. Zhu, "Average Torque Separation in Permanent Magnet Synchronous Machines Using Frozen Permeability," *IEEE Trans. Magn.*, vol. 49, no. 3, pp. 1202 - 1210, Mar. 2013.
- [23] S. Stipetić, D. Žarko and M. Popescu, "Ultra-fast axial and radial scaling of synchronous permanent magnet machines," *IET Electric Power Applications*, vol. 10, no. 7, pp. 658-666, 8 2016.
- [24] A. A. Rockhill, T. A. Lipo, "A Generalized Transformation Methodology for Polyphase Electric Machines and Networks," in *Electric Machines & Drives Conference (IEMDC), 2015 IEEE International*, Coeur d'Alene, Idaho, USA, pp. 1-8, 10-13 May 2015.
- [25] T. Miller, *Brushless Permanent Magnet and Reluctance Motor Drives*, Oxford: Clarendon Press, 1989.
- [26] Shin-Etsu Chemical Co., Ltd., "N36Z Nd-Fe-B Magnet Demagnetization Curves at Elevated Temperatures," Apr. 2016. [Online]. Available: <http://www.shinetsu-rare-earth-magnet.jp/e/>.